Communications in Applied and Industrial Mathematics, DOI: 10.1685/journal.caim.370
ISSN 2038-0909, e-370

A computational model for biomass growth simulation in tissue engineering

Paola Causin[1], Riccardo Sacco[2]

[1] *Dipartimento di Matematica "F. Enriques", Università degli Studi di Milano, Italy*
paola.causin@unimi.it

[2] *Dipartimento di Matematica "F. Brioschi", Politecnico di Milano, Italy*
riccardo.sacco@polimi.it

Communicated by Jean-Frédéric Gerbeau

Abstract

This article deals with computational modeling of tissue growth under interstitial perfusion inside a polymeric scaffold-based bioreactor. The mathematical model is the result of the application of the volume averaging technique to the fluid, nutrient and cellular subsystems, and is capable to account for the temporal evolution of local matrix porosity, as the sum of a time-invariant component (the porosity of the uncellularized polymer scaffold) and a time-dependent component (due to the growing biomass). The solution algorithm is based on a block Gauss-Seidel iteration procedure that allows to reduce each time level of the simulated culture period into the successive solution of linearized subproblems, whose numerical approximation is carried out using stable and convergent finite elements. Numerical simulations are carried out to investigate the role of the design porosity of the scaffold on nutrient delivery and biomass production.

Keywords: `Tissue engineering, artificial cartilage, computational model, multi-physics and multi-scale problems, interstitial perfusion, bioreactor, fluid dynamics, mass transport, numerical simulation, finite element method.`

AMS Subject Classification: `05A16, 65N38, 78M50`

1. Introduction.

In this article, we deal with the mathematical modeling and the numerical simulation of *in vitro* tissue growth, with application to regeneration of articular cartilage, the smooth white tissue lining the surface of all the diarthrodial joints in the body, critical in the movement of one bone against another. In particular, we consider tissue growth inside a scaffold made of

Received 2010 12 14, Accepted 2011 04 04, Published 2011 09 07.

a polymeric porous foam immersed in a bioreactor device under interstitial perfusion. Tissue Engineering (TE) techniques based on the interstitial flow of the culture medium have been recognized to provide a proper biophysical microenvironment to cells [1–3] compared to both static culture and surface perfusion systems. Dynamic perfusion has been found to be particularly effective in improving the delivery of nutrients in the densely cell populated areas of the construct, promoting cell proliferation and up-regulating the synthesis of matrix proteins specific to cartilaginous tissue, such as collagens and glycosaminoglycan (GAG) [4–13]. Fig. 1 gives a schematic picture of the multi-scale/multi-physics structure of the phenomena occurring inside a porous matrix for tissue engineering applications.

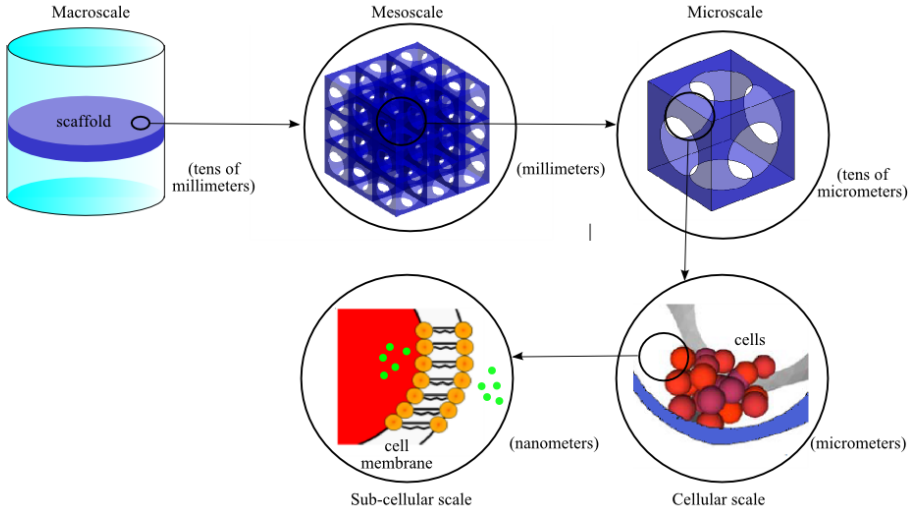

Figure 1. Multiple scale phenomena take place in a bioreactor system, spanning from some tens of millimeters to nanometers.

Based on such a representation, the engineered tissue can be analyzed at different levels of detail, according to the following definitions:

- Macroscale level: it is the scale at which the perfused scaffold is treated as a continuum and at which the Bioengineer sets the control parameters (inlet velocity, pressure drop). Its characteristic length is of the order of some millimeters.
- Mesoscale level: it is the scale corresponding to a collection of a few pores of the scaffold. Its characteristic length spans from hundreds of microns to millimeters.
- Microscale level: it is the scale of the single pore of the polymeric

DOI: 10.1685/journal.caim.370

scaffold, of nominal diameter of 100μm.
- Cellular level: it is the scale at which cells cannot be treated as a continuum, but must be treated as single discrete entities. Its characteristic length is of the order of microns.
- Sub-cellular scale level: it is the scale accounting for all the mass transport and reaction processes that occur at the single cell membrane level. Its characteristic length is of the order of some nanometers.

From the mathematical viewpoint, several computational studies analyze the problem focusing only on the Macroscale level. Namely, such studies concern the numerical evaluation of the fluid-dynamical field and/or of the nutrient (oxygen or glucose) distribution in the construct as if the system were homogeneous (see, *e.g.*, [14–16]). However, the environment in a TE construct is a composite constituted of a collection of biomass, interstitial fluid, polymeric scaffold. Multiphase models allow explicit consideration of these interactions. Each constituent is considered as a distinct phase within the multiphase system with corresponding constitutive laws and interactions with neighboring phases; the inherent complexity of this approach can be conveniently reduced by an averaging process, yielding a single equation which holds uniformly in the material. Derivation of multiphase models applied to a wide range of problems in computational biology has been given extensive treatment by many authors, including for example [17–20]. In the series of papers by Galban & Locke (see [21] and references therein), a two phase (fluid and biomass) model for cell growth and nutrient diffusion in a polymer scaffold with no perfusion is presented. A single, averaged reaction-diffusion equation for the nutrient concentration in the two phase system is derived using the volume-averaging method of [19,22] and the effective diffusion coefficient and reaction rate are calculated as a function of the local cell volume fraction. This latter is determined (as a function of time) by considering a cell population balance equation. In the paper by Chung et al. [23] a two–phase (fluid and biomass) model analogous to the one of [21] is proposed, with the inclusion of a self–consistent computation of the fluid-dynamic field via an averaged Stokes–Brinkman model. To reflect the fact that cell growth into the scaffold reduces the effective pore size, Chung et al. propose to include the dependency on the cell volume fraction via a Carman-Kozeny type relation for the permeability.

The present paper takes depart from our earlier work [24], where we have proposed a macroscopic model obtained from volume averaging procedures applied to a three-phase (fluid-biomass-scaffold) model. Fluid perfusion and cell proliferation have been taken into account as well, as in [23].

With respect to [24], we address here the complete derivation of the model with emphasis on characteristic nondimensional numbers. Moreover, we present novel numerical simulations, focused on a parametric study of the effect of the scaffold porosity.

The paper is organized as follows: in Section 2 we present the mathematical model, a system of non-linearly coupled partial differential equations which describes, at the macroscopic level, fluid flow throughout the porous scaffold matrix, nutrient mass transfer and cellular proliferation and metabolism; in Sect. 3 we describe the computational algorithm used to to reduce each time level of the simulated culture period into the successive solution of linearized sub-problems, whose numerical approximation is carried out using stable and convergent finite elements [25]. The computational procedure is then used in Sect. 4 to carry out a parametric study, as a function of the uncellularized scaffold porosity, of dynamically perfused tissue growth in realistic geometries [26].

2. Mathematical model.

In the following, we describe the mathematical model adopted for the description of tissue growth in the porous construct. The main mathematical tool we use is the Volume Averaging Method (VAM) [19,21,22], which is applied separately to the three phases composing the bio–hybrid device, namely, the interstitial fluid, the nutrient substance (glucose) and the biomass. The use of the VAM allows to upscale to a macroscopic level the local properties of each subsystem through the introduction of *effective* coefficients (nutrient diffusivity and medium porosity).

2.1. *Flow perfusion with Brinkman frictional correction.*

Let $\Omega_{sc} \in \mathbb{R}^d$, $d = 1, 2, 3$, be a bounded open domain, fixed in time, representing a porous scaffold, and $T > 0$ the temporal duration of the cell culture process. A schematical representation of a 2D vertical cross-section of a typical scaffold, of width W and thickness H, is shown in Fig. 2.
In order to carry out the upscaling of interstitial flow throughout the porous scaffold matrix progressively filled with growing biomass, we associate with every $\mathbf{x} \in \Omega_{sc}$ an arbitrary, but fixed in time, representative elementary volume (REV) $V = V(\mathbf{x})$ having $\mathbf{x}$ as its centroid and such that the characteristic size of V is the order of the union of some pores, roughly corresponding to the Mesoscale. Thus, V is "small" enough with respect to the characteristic length of the macroscopic scale and "big enough" with respect to the characteristic length of the cellular scale. We denote by V_{fl}, V_{sc} and V_{bio} the portions of V occupied by the perfusion fluid, by the scaf-

DOI: 10.1685/journal.caim.370

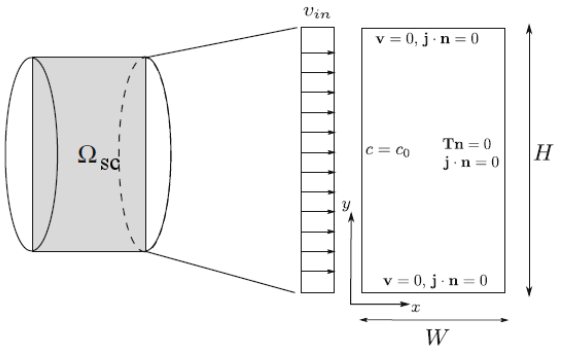

Figure 2. Schematical geometry of the scaffold and boundary conditions. Perfusion medium carrying nutrient is flowing from left to right.

fold porous structure and by the growing biomass, respectively, satisfying at each fixed time level $t \in [0, T]$ the relation

$$V(\mathbf{x}) = V_{sc} + V_{fl}(\mathbf{x}, t) + V_{bio}(\mathbf{x}, t).$$

Clearly, being V and V_{sc} time-invariant volumes, we expect V_{bio} to increase along with the culture process, and, accordingly, V_{fl} to decrease. Associated with the above geometrical quantities, we let $\epsilon_s := V_{sc}/V$ and $\epsilon_{bio} := V_{bio}/V$ be the volumetric fractions occupied by the scaffold porous structure and by the biomass (cells + extracellular matrix), respectively, and we define the space and time–dependent scaffold porosity

$$\phi(\mathbf{x}, t) := V_{fl}/V = 1 - (\epsilon_s + \epsilon_{bio}(\mathbf{x}, t)). \tag{1}$$

The geometrical description of the scaffold porosity, accounting for the background (uncellularized) polymer solid structure, is motivated by the data of [26,27], where the range of variation for ϕ was $59 - 89\%$, with a reference value of 77%. A parametric study of the effects of the variations of the scaffold fraction ϵ_s on the interstitial cell growth process will be discussed in the numerical experiments of Sect. 4. Finally, we indicate by $\mathbf{v}_{fl}^{point}$ the point fluid velocity, by $\mathbf{v}_{fl} := \int_{V_{fl}} \mathbf{v}_{fl}^{point}/V_{fl}$ the average intrinsic velocity (i.e., the average fluid velocity over the *sole* fluid volume), and by $\mathbf{v} := \int_{V_{fl}} \mathbf{v}_{fl}^{point}/V = \phi \mathbf{v}_{fl}$ the Darcy fluid velocity (i.e., the average fluid velocity over the *whole* REV).

Then, we apply the VAM over the REV to the point balance equations for mass and momentum [28–31], and obtain the following system of macroscopic equations for interstitial fluid flow in Ω_{sc}:

$$\partial_t \phi + \operatorname{div} \mathbf{v} = 0, \tag{2a}$$

$$\rho\Big(\partial_t \mathbf{v} + \operatorname{div}\left((\mathbf{v}\times\mathbf{v})/\phi\right)\Big) = \operatorname{div}\mathbf{T}(\mathbf{v},P) + \mathbf{b}(\mathbf{v},\phi) + \rho\mathbf{f}, \tag{2b}$$

$$\mathbf{T}(\mathbf{v},P) := 2\mu\,\boldsymbol{\varepsilon}(\mathbf{v}) - PI, \tag{2c}$$

$$\mathbf{b}(\mathbf{v},\phi) := -\mu\phi K_D^{-1}(\phi)\mathbf{v}, \tag{2d}$$

where $\boldsymbol{\varepsilon}(\mathbf{v})$ denotes the symmetric gradient of $\mathbf{v}$, while $P = \phi P_{fl}$ is the Darcy fluid pressure (i.e., after volume averaging over the whole REV), $\mathbf{T}$ is the associated fluid stress tensor, μ being the fluid dynamic viscosity, and $\mathbf{f}$ is a force per unit mass and unit volume in a fluid having density equal to ρ.

Eq. (2a) represents mass conservation for a pseudo-compressible fluid, the mass source being due to the fact that the fluid volume fraction is *not* constant in time (notice, that, instead the REV does not vary in time). Eq. (2b) represents momentum conservation: we see that the process of volume averaging has introduced an extra term $\mathbf{b}$, which expresses, via the permeability defined below, the total drag force per unit volume exerted on the fluid particles by the biomass and scaffold surfaces. As the characterization of the frictional term would require the pointwise knowledge of the microscopic normal stress in V, a closure relation for $\mathbf{b}$ is needed to end up with a computable model. Such closure relation is provided by Eq. (2d), which represents the Brinkman's correction to fluid motion due to the presence of porous matrix structure, where the Darcy permeability K_D is expressed by the Carman-Kozeny relation [19,30,32]

$$K_D(\phi) := K_p \frac{\phi^3}{(1-\phi)^2}, \tag{3}$$

the Kozeny constant K_p being a reference permeability referred to the uncellularized scaffold. Eq. (3) is valid, in principle, for a porous matrix structure composed of a dilute random array of spherical particles. However, it has been shown to be able to satisfactorily represent a wider variety of situations (see for example the tests carried out in [33], Ch. 6). Moreover, we observe that this formula is proposed here as a preliminary attempt, in lack of a rigourous theoretical foundation in the field object of the present work.

DOI: 10.1685/journal.caim.370

2.2. *Nutrient mass transport.*

In order to carry out the upscaling of microscale mass transport phenomena, we consider an arbitrary, but fixed, REV $V \subset \Omega_{sc}$ whose spatial resolution is far below the structural heterogeneities characterizing the upper scale level (i.e., the scaffold porosity). This allows us to define by $V_\beta = V_\beta(\mathbf{x}, t)$ and $V_\sigma = V_\sigma(\mathbf{x}, t)$ the two portions of V associated with the fluid (β) and solid (biomass+scaffold) (σ) phases, in such a way that $V = V_\beta(\mathbf{x}, t) + V_\sigma(\mathbf{x}, t)$. Then, denoting by $c^{micro} = c^{micro}(\mathbf{x}, t)$ the microscopic nutrient concentration, and setting $c_\beta := \int_{V_\beta} c^{micro}/V_\beta$ and $c_\sigma := \int_{V_\sigma} c^{micro}/V_\sigma$ the average intrinsic nutrient concentrations in the two phases, we can define the average nutrient concentration at the Microscale as

$$c := \frac{\int_V c^{micro}}{V} = \frac{\int_{V_\beta} c^{micro} + \int_{V_\sigma} c^{micro}}{V} = \phi c_\beta + \epsilon_{bio} c_\sigma. \tag{4}$$

Notice that in Eq. (4) we have used the fact that the scaffold is impermeable to nutrient mass transport, as reflected by the fraction ϵ_{bio} weighting c_σ. Before carrying out the upscaling, we need to look at a finer level, the sub-cellular level, in order to account for protein-mediated reactions regulating nutrient mass transport across the cellular membrane. Because of the extremely small thickness of the membrane (of the order of nanometers), it is reasonable to assume that transmembrane phenomena occur on a much faster time-scale than in the intra and extra-cellular phases, so that the following *local mass equilibrium* relation holds [22]

$$c_\sigma = K_{eq} c_\beta, \tag{5}$$

where K_{eq} is a suitable equilibrium coefficient. Using (5) into (4), we express the average nutrient concentration in the biomass in terms of the sole average fluid nutrient concentration as $c = (\phi + K_{eq}\epsilon_{bio})c_\beta$. Then, we apply the VAM over the REV to the sub-cellular balance equations for mass transport between β and σ-phases, and we obtain the following system of macroscopic equations for interstitial nutrient mass transport in Ω_{sc}:

$$\partial_t\big((\phi + K_{eq}\epsilon_{bio})c_\beta\big) + \operatorname{div} \mathbf{j}_{nutr}(c_\beta, \mathbf{v}) = g_{nutr}(c_\beta, \epsilon_{bio}), \tag{6a}$$

$$\mathbf{j}_{nutr}(c_\beta, \mathbf{v}) := -D_{eff}\nabla c_\beta + \mathbf{v} c_\beta, \tag{6b}$$

$$D_{eff} := D_\beta \frac{3k - 2\phi(k-1)}{3 + \phi(k-1)}, \qquad k := K_{eq}\frac{D_\sigma}{D_\beta}, \tag{6c}$$

$$g_{nutr}(c_\beta, \epsilon_{bio}) = -\frac{R_m \epsilon_{bio} c_\beta}{K_m + c_\beta}. \tag{6d}$$

The equation system (6) expresses the dynamical macroscopic nutrient mass balance at every point of Ω_{sc}. The nutrient mass flux $\mathbf{j}_{nutr}$ comprises a diffusive contribution according to Fick's law and an advective contribution due to fluid perfusion, while the reaction source term g_{nutr}, nonlinearly depending on the average nutrient concentration in the β-phase, is the rate of nutrient mass consumption according to the Michaelis-Menten model [22]. By inspection on Eq. (6c), we see that the process of volume averaging has introduced an effective diffusion coefficient D_{eff} (described by Maxwell model [22]), which expresses the upscale contribution of the sub-cellular scale geometry on the macroscopic transport process. It can be checked that relation (6c) always yields a strictly positive quantity in correspondance of any value of $k \in [0, +\infty]$ and $\phi \in [0, 1]$. Moreover, we have

$$\lim_{\phi \to 0^+} D_{eff} = K_{eq} D_\sigma = D_\sigma, \qquad \lim_{\phi \to 1^-} D_{eff} = D_\beta,$$

consistently with the fact that in the first case there is no extra-cellular phase, while in the second case there is no intra-cellular phase.

2.3. *Cell growth dynamics.*

In order to carry out the upscaling of microscale cellular proliferation and metabolism phenomena, we follow [21,34] and apply the VAM to the conservation of cell mass associated with a volume V_σ, contained within a REV $V \subset \Omega_{sc}$, obtaining the following system of macroscopic equations that describes interstitial growth of tissue cells in Ω_{sc}:

$$\partial_t \epsilon_{bio} + \operatorname{div} \mathbf{j}_{cell}(\epsilon_{bio}) = g_{cell}(c_\beta, \epsilon_{bio}), \tag{7a}$$

$$\mathbf{j}_{cell}(\epsilon_{bio}) := -D_{cell} \nabla \epsilon_{bio}, \tag{7b}$$

$$g_{cell}(c_\beta, \epsilon_{bio}) = \Big(\frac{R_g c_\beta}{c_\beta + \rho_{cell} \frac{K_c}{K_{eq}} \epsilon_{bio}} - R_d \Big) \epsilon_{bio}. \tag{7c}$$

The equation system (7) expresses the dynamical macroscopic cell material balance at every point of Ω_{sc}. The diffusive cell mass flux $\mathbf{j}_{cell}$ accounts for cell randow walk throughout the porous matrix, while the reaction source term g_{cell}, nonlinearly depending on the cell volume fraction ϵ_{bio}, accounts for the competing mechanisms of cell growth R_g and cell apoptosis R_d according to the modified Contois model [35].

DOI: 10.1685/journal.caim.370

2.4. *Nondimensionalization and simplification of the model.*

In this section, we write the three equation systems (2), (6) and (7) in non–dimensional form, in order to single out characteristic numbers whose order of magnitude can be used to simplify in a rigorous way the model.

Given a generic variable u, we associate with u a scaling factor $\overline{u}$, in such a way that $u/\overline{u}$ is the non–dimensional variable corresponding to u. We define four independent scaling factors (SF): $\overline{x}$ (space SF), $\overline{t}$ (time SF), $\overline{u}$ (velocity SF) and $\overline{c}$ (concentration SF). We set $\overline{x} := H$ and $\overline{t} := R_g^{-1}$, because we expect the maximum cell growth rate to be the characteristic time regulating the overall process. We also set $\overline{u} := U_{in}$ and $\overline{c} := c_{in}$, U_{in} and c_{in} being the maximum perfusion velocity and nutrient concentration at the inlet section of the scaffold domain, respectively. For notational simplicity, we continue to use in the following the same symbol to indicate the corresponding non–dimensional quantity, unless otherwise specified.

Then, the non–dimensional equations for fluid perfusion in the scaffold read:

$$
\begin{aligned}
&\boxed{\delta_v}\,\partial_t\phi + \operatorname{div}\mathbf{v} = 0,\\
&\operatorname{Re}\operatorname{Da}\Big(\delta_v\partial_t\mathbf{v} + \operatorname{div}\big((\mathbf{v}\times\mathbf{v})/\phi\big)\Big) = \operatorname{div}\widetilde{\mathbf{T}}(\mathbf{v},p) - \chi(\phi)^{-1}\mathbf{v},\\
&\widetilde{\mathbf{T}}(\mathbf{v},p) := 2\operatorname{Da}\boldsymbol{\varepsilon}(\mathbf{v}) - pI, \qquad \chi(\phi) := \phi^2/(1-\phi)^2,
\end{aligned}
\tag{8}
$$

where $p := (P - (-\rho g\mathbf{e}_y)\cdot\mathbf{x})/\overline{p}$ is the piezometric pressure, g being gravity acceleration, $\mathbf{e}_y$ the unit vector oriented from bottom to top in Fig. 2, and $\overline{p} := \mu\overline{u}\,\overline{x}/K_p$, respectively. The quantities $\operatorname{Re} := \overline{u}\,\overline{x}/\nu$ and $\operatorname{Da} := K_p/\overline{x}^2$ are the Reynolds and Darcy numbers, $\nu := \mu/\rho$ being the kinematic fluid viscosity, while the quantity $\delta_v := (\overline{x}/\overline{t})/\overline{u}$ is the ratio between the characteristic velocity of cell growth and the characteristic velocity of the fluid in the scaffold.

The non–dimensional equations for nutrient mass transport are:

$$
\begin{aligned}
&\boxed{\delta_D}\,\partial_t\big((\phi + K_{eq}\epsilon)c\big) + \operatorname{div}\mathbf{j}_{nutr}(c,\mathbf{v}) = -\frac{\widehat{R}_m\epsilon c}{c+\widehat{K}_m},\\
&\mathbf{j}_{nutr}(c,\mathbf{v}) := -\widehat{D}_{eff}\nabla c + \operatorname{Pe}_{glob}\mathbf{v}, \qquad \widehat{D}_{eff} := \frac{3k - 2\phi(k-1)}{3+\phi(k-1)},
\end{aligned}
\tag{9}
$$

where c and ϵ shortly denote the non–dimensional nutrient concentration in the fluid phase and the biomass volume fraction, respectively, and having set $\widehat{R}_m := R_m/(\overline{c}D_\beta/\overline{x}^2)$ and $\widehat{K}_m := K_m/\overline{c}$. The quantity $\operatorname{Pe}_{glob} := (\overline{u}\,\overline{x})/D_\beta$ is the Peclèt number associated with the whole scaffold domain, while the quantity $\delta_D := (\overline{x}^2/D_\beta)/\overline{t}$ is the ratio between the characteristic diffusion

time of the nutrient in the fluid and the time-scale of the reactions governing cell growth in the scaffold.

The non–dimensional equations for the cell volume fraction are:

$$\begin{aligned} &\boxed{1}\,\partial_t \epsilon + \operatorname{div} \mathbf{j}_{cell}(\epsilon) = \Big(\frac{c}{c+\eta\epsilon} - \widehat{R}_d\Big)\epsilon, \\ &\mathbf{j}_{cell}(\epsilon) := -\widehat{D}_{cell}\nabla\epsilon_{bio}, \qquad \widehat{D}_{cell} := \frac{D_{cell}}{\overline{x}^2/\overline{t}}, \end{aligned} \tag{10}$$

where $\eta := (K_c\rho_{cell})/(K_{eq}\overline{c})$ and $\widehat{R}_d := R_d/\overline{t}^{-1}$. The quantity $\widehat{D}_{cell}$ is the ratio between the time-scale of cell growth reactions and the time-scale of cell random walk through the porous structure of the scaffold.

It is now relevant to numerically evaluate the relative weight of the constants δ_v and δ_D compared to $\delta_c := 1$, in order to see whether some model reduction can be carried out. With this aim, we summarize in Tab. 1 the values of the geometrical and bio-physical parameters as proposed in [23] and in the references cited therein.

Table 1. Model parameters.

Symbol	Meaning	Value	Units
W	Scaffold width	1	cm
H	Scaffold thickness	0.3	cm
U_{in}	Maximum perfusion velocity	50	$\mu m\, s^{-1}$
c_{in}	Nutrient concentration at scaffold inlet	4.5×10^{-3}	$g\, cm^{-3}$
R_g	Maximum cell growth rate	1.6×10^{-5}	s^{-1}
μ	fluid dynamic viscosity	8.3×10^{-3}	$g\, cm^{-1}\, s^{-1}$
ρ	fluid density	0.893	$g\, cm^{-3}$
K_p	Carman-Kozeny constant	10^{-2}	cm^2
D_β	Nutrient diffusivity in the β-phase	1.0×10^{-5}	$cm^2\, s^{-1}$
D_σ	Nutrient diffusivity in the σ-phase	0.75×10^{-5}	$cm^2\, s^{-1}$
K_{eq}	Local mass equilibrium coefficient	0.1	Adimensional
K_m	Saturation coefficient	6.3×10^{-5}	$g\, cm^{-3}$
R_m	Maximum nutrient uptake rate	8×10^{-6}	$g\, cm^{-3}\, s^{-1}$
D_{cell}	Cellular diffusivity due to random walk	1.7×10^{-10}	$cm^2\, s^{-1}$
R_d	Cell apoptosis rate	3.3×10^{-7}	s^{-1}
K_c	Contois saturation coefficient	0.154	Adimensional
ρ_{cell}	Specific cell density	0.182	$g\, cm^{-3}$

Using the tabulated values of the parameters, we have $\delta_v = 9.6 \times 10^{-4}$ and $\delta_D = 0.14$, so that the term $\delta_v \partial_t \phi$ in Eq. $(8)_1$ can be safely neglected. Moreover, we also compute Re $\simeq 0.16$ and Da $\simeq 0.11$, so that also the inertial terms in the momentum balance equation $(8)_2$ can be neglected. Eventually, we notice that $\widehat{D}_{cell} \simeq 1.18 \times 10^{-4}$, indicating that cell growth reactions occur on a much faster time-scale than cell random walk.

DOI: 10.1685/journal.caim.370

Based upon the above considerations, the simplified model for biological tissue growth under fluid perfusion in a scaffold reads:

$$
(11)\quad \begin{cases} \operatorname{div}\mathbf{v} = 0, \\ \operatorname{div}\widetilde{\mathbf{T}}(\mathbf{v},p) - \chi(\phi)^{-1}\mathbf{v} = \mathbf{0}, \\ \widetilde{\mathbf{T}}(\mathbf{v},p) := 2\mathrm{Da}\,\boldsymbol{\varepsilon}(\mathbf{v}) - pI, \qquad \chi(\phi) := \phi^2/(1-\phi)^2, \end{cases}
$$

$$
\begin{cases} \delta_D\,\partial_t\big((\phi + K_{eq}\epsilon)c\big) + \operatorname{div}\mathbf{j}_{nutr}(c,\mathbf{v}) = -\dfrac{\widehat{R}_m\epsilon c}{c+\widehat{K}_m}, \\ \mathbf{j}_{nutr}(c,\mathbf{v}) := -\widehat{D}_{eff}\nabla c + \mathrm{Pe}_{glob}\mathbf{v}, \qquad \widehat{D}_{eff} := \dfrac{3k - 2\phi(k-1)}{3+\phi(k-1)}, \end{cases}
$$

$$
\begin{cases} \partial_t\epsilon = \Big(\dfrac{c}{c+\eta\epsilon} - \widehat{R}_d\Big)\epsilon. \end{cases}
$$

3. Computational algorithm.

In this section, we illustrate the fixed-point map for system linearization, the time-marching procedure and the finite element approximation of the linearized differential subproblems.

3.1. *Linearization and time-advancing.*

Model (11) is a system of nonlinearly coupled PDEs for the set of dependent variables $\mathbf{v}$, p, c and ϵ, and must be solved in the scaffold domain Ω_{sc} supplied with suitable initial and boundary conditions, as described in Sect. 4. This requires to linearize the fully coupled system in order to end up with a sequence of differential subproblems that are easier to treat in a computational algorithm. With this aim, let us divide the temporal interval $[0,\,T]$ into $N_T \geq 1$ time levels of length $\Delta t := T/N_T$, such that $t_n := n\Delta t$, $n = 0,\ldots,N_T$ and, for a generic function $u(\mathbf{x},t)$, set $u_n := u(\mathbf{x},t_n)$. Then, given the initial data $\mathbf{v}_0$, c_0 and ϵ_0, for each $n = 1,\ldots,N_T$ solve the following sequence of *linear* differential sub-problems:

$$
\text{(12a)}\qquad \begin{cases} \operatorname{div}\mathbf{v}_n = 0, \\ \operatorname{div}\widetilde{\mathbf{T}}(\mathbf{v}_n,p_n) - \chi(\phi_{n-1})^{-1}\mathbf{v}_n = \mathbf{0}, \end{cases}
$$

$$
\text{(12b)}\qquad \begin{aligned} &\operatorname{div}\mathbf{j}_{nutr}(c_n,\mathbf{v}_n) + \Big(\delta_D\frac{(\phi_{n-1} + K_{eq}\epsilon_{n-1})}{\Delta t} + \frac{\widehat{R}_m\epsilon_{n-1}}{c_{n-1}+\widehat{K}_m}\Big)c_n \\ &= \delta_D\frac{(\phi_{n-1} + K_{eq}\epsilon_{n-1})c_{n-1}}{\Delta t}, \end{aligned}
$$

$$\text{(12c)} \qquad \Big(\frac{1}{\Delta t} + \widehat{R}_d\Big)\epsilon_n = \Big(\frac{1}{\Delta t} + \frac{c_n}{c_n + \eta\epsilon_{n-1}}\Big)\epsilon_{n-1}.$$

Time advancing from time level t_{n-1} to time level t_n is carried out using the Backward Euler method, because of its inconditional stability and ease of implementation, while system inner decoupling is carried out using a fixed-point iteration of block Gauss-Seidel form. Precisely, for a given scaffold porosity ϕ_{n-1}, the part of model (11) describing fluid perfusion throughout the scaffold is a *linear* Stokes-Brinkman problem for the pair ($\mathbf{v}$, p). This is reflected into Eq. (12a) that constitutes the first step of the algorithm, and provides the pair ($\mathbf{v}_n$, p_n). Plugging ϕ_{n-1} and $\mathbf{v}_n$ into the equation of mass nutrient delivery in model (11), however, would yield an advection-diffusion problem for c with *non-linear* reaction terms. Eq. (12b) is a suitable linearization of such a problem, constructed in such a way that the absorption and production terms are positive given functions. This ensures, in turn, a maximum principle to hold for the solution c_n (see [36]), which can be proved to be positive in Ω_{sc} as physically expected. The same philosophy underlies Eq. (12c), that is a linear diffusion-reaction problem for ϵ_n, which can be proved to be positive in Ω_{sc}, again as physically expected. A flow-chart of the computational algorithm for cell growth simulation is shown in Fig. 3, where the quantities on the left of each arrow are input data to the successive equation block in the chart, and the quantities on the right are the output of the previous equation block in the chart.

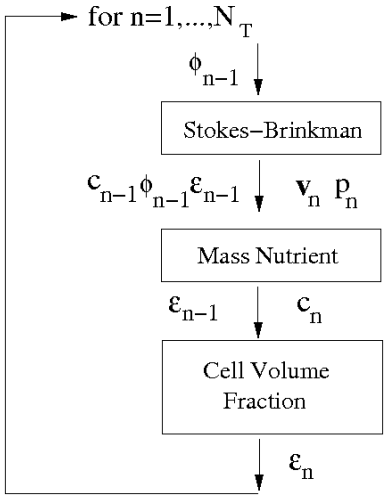

Figure 3. Flow-chart of the computational algorithm.

DOI: 10.1685/journal.caim.370

3.2. *Finite element approximation.*

In this section, we address the issue of the numerical discretization, using the Galerkin Finite Element Method (GFEM) [25], of each of the linearized differential subproblems to be solved at each time level in the functional iteration (12). With this aim, we introduce a triangulation $\mathcal{T}_h$ of Ω_{sc} made of regular open simplices K (intervals in 1D, triangles in 2D and tetrahedra in 3D) [37], such that $\Omega_{sc} = \cup_{K\in\mathcal{T}_h} K$. Then, the approximation of (12a) is carried out using the Taylor-Hood finite element pair [38]. This choice satisfies the inf-sup compatibility condition (see [25], Chapt. 9) and avoids the onset of spurious pressure modes. As for subproblems (12b) and (12c), both can be written in the general form of a linear diffusion-advection-reaction equation:

$$\begin{aligned} &\mathrm{div}\mathbf{F}(u;\boldsymbol{\beta}) + \sigma\, u = f, \\ &\mathbf{F}(u;\boldsymbol{\beta}) : -\mathcal{D}\nabla u + \boldsymbol{\beta} u, \end{aligned} \tag{13}$$

where $\boldsymbol{\beta}$ is a given divergence-free advective field, while σ and f are given positive functions. The approximation of (13) is carried out using a standard SUPG formulation with piecewise linear continuous finite elements (see [39,40]). This choice ensures a numerically stable solution even in the case of a local Peclèt number > 1.

4. Simulation results and discussion.

In this section we use the computational model proposed above to simulate biomass growth in the polymer-based scaffolds experimentally investigated in [26,27,41]. A μCT image of a detail of the bioreactor porous matrix is shown in Fig. 4 (left), while Fig. 4 (right) illustrates a schematics of the simplified geometrical model used in computations to represent the whole scaffold matrix as a periodical "honey-comb" repetition of a cubic "unit cell" intersected by a sphere. Referring to Fig. 5 (left), we denote by H and R the size of the unit cell and the radius of the intersecting sphere, respectively, and we set $h := R - H/2$. To compute the porosity of the uncellularized scaffold we need to evaluate the volumetric fraction V_{sc} that is occupied by the solid porous matrix within the total volume of the unit cell $V = H^3$. A simple geometrical computation shows that

$$V_{sc} = H^3 - \left(\frac{4\,\pi}{3}R^3 - 6\frac{\pi}{3}h^2\,(3R-h)\right),$$

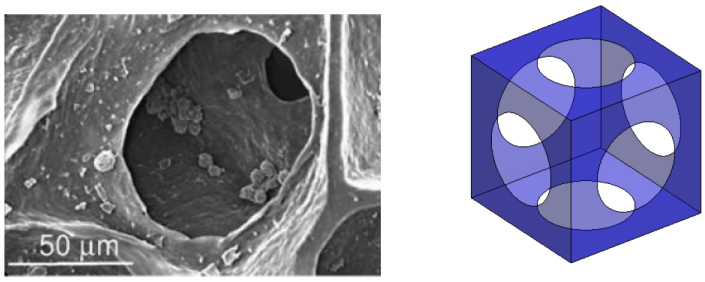

Figure 4. Left: μCT image of a representative construct at the single pore level; right: simplified geometrical model.

from which, introducing the dimensionless parameter $\lambda := R/(H/2)$ such that $1 < \lambda < \sqrt{2}$, we obtain

$$\epsilon_s(\lambda) = \frac{V_{sc}}{V} = \left(1 + \frac{\pi}{4}\right) + \frac{\pi}{3}\lambda^3 - \frac{3\pi}{4}\lambda^2.$$

The graph of ϵ_s as a function of λ is depicted in Fig. 5 (right), indicating that scaffold porosity dramatically decreases from almost 50% (corresponding to $\lambda = 1$) to almost 2% (corresponding to $\lambda = \sqrt{2}$).

As the main focus of our analysis is the investigation of the role of the scaffold porosity ϵ_s in determining the effectiveness of nutrient (glucose) delivery to the cellular environment, and, consequently, in driving cell metabolism and biomass production, we clearly expect the above reduction of void fraction to reflect into a strong reduction of nutrient delivery efficiency and, consequently, biomass production. To assess this conjecture, we have implemented the computational algorithm of Sect. 3 in a Matlab routine, and run the code with the following input data: $W = 1\,cm$, $H = 0.307\,cm$, $c_0 = 4.5 \cdot 10^{-3}\,g\,cm^{-3}$ and $U_{in} = 3.5\,\mu m\,s^{-1}$. The finite element triangulation is of Friedrichs-Keller type, with triangle edge sizes

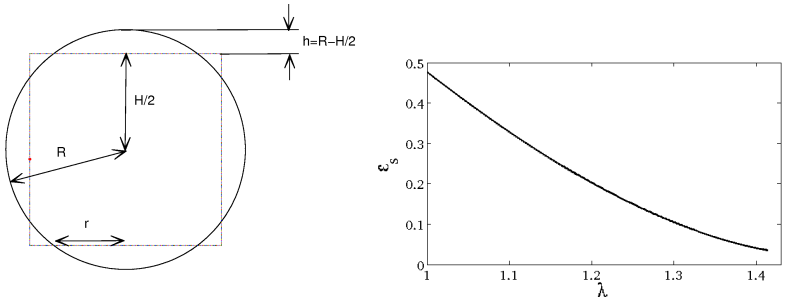

Figure 5. Left: two-dimensional section of the unit cell; right: graph of ϵ_s as a function of the dimensionless parameter λ.

DOI: 10.1685/journal.caim.370

$h_x = W/20$ and $h_y = H/20$ in the x and y directions, respectively. The final simulated culture time is $T = 60$ days and $\Delta t = 12$ hours. The results of the simulation are shown in Fig. 6 and 7, where the x-and y coordinates are normalized to $\overline{x} = H$. As expected, glucose delivery to deeper scaffold

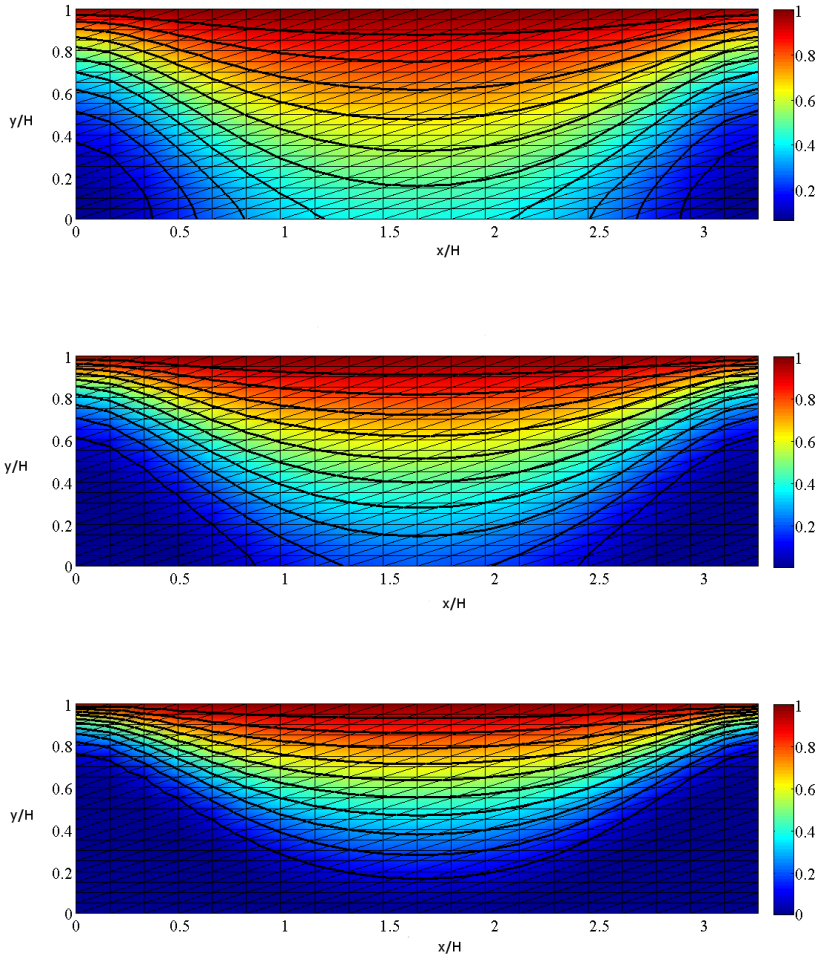

Figure 6. Nutrient concentration (normalized to c_0) as a function of $\epsilon_s(\lambda)$. Top: $\lambda = 1$, middle: $\lambda = 1.138$, bottom: $\lambda = 1.345$.

sections is strongly inhibited as the solid porous volume fraction increases, and the same phenomenon occurs with biomass production which is mainly confined to the scaffold region close to the inlet section where the maximum amount of nutrient is available. Inhibition of nutrient delivery and biomass

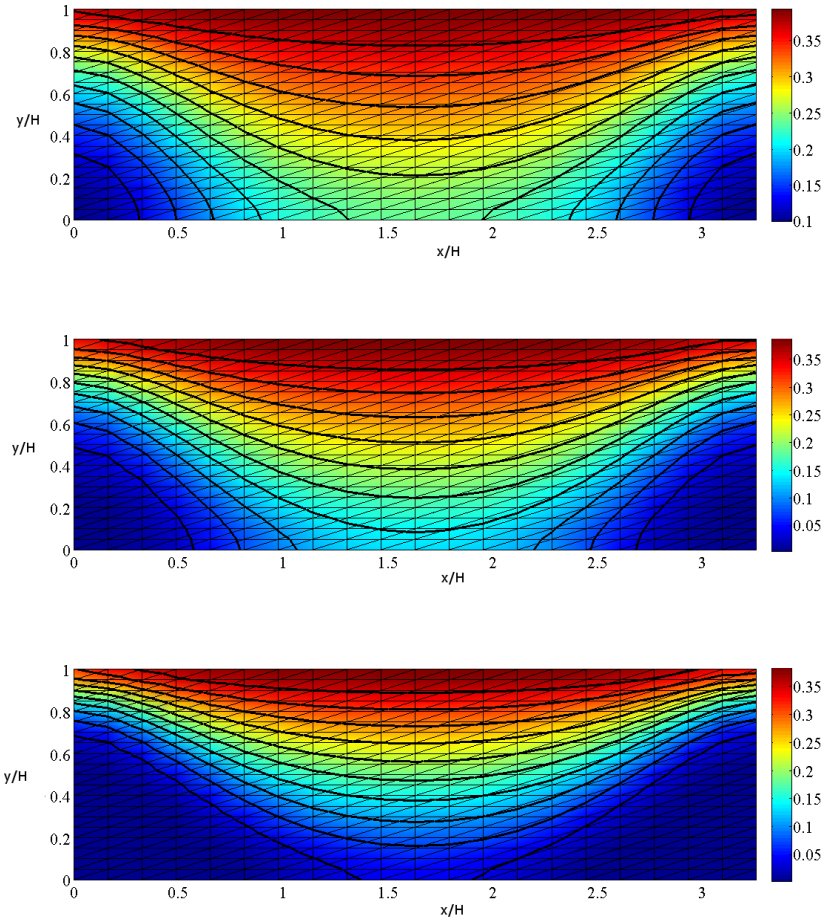

Figure 7. Biomass volume fraction as a function of $\epsilon_s(\lambda)$. Top: $\lambda = 1$, middle: $\lambda = 1.138$, bottom: $\lambda = 1.345$.

production due to the increase of solid volume fraction is even more noticeable in the graphs of Fig. 8 where the maximum, minimum and average values of c and ϵ over Ω_{sc} are plotted as a function of ϵ_s. We observe that for (almost) every scaffold porosity, there exist sub–regions of the device where the nutrient concentration is very low (cf. the minimum curves), this being an indication of non–optimal nutrient perfusion. As for the average curves, the trend is almost linear with scaffold porosity, this being an interesting indication for design purposes that, however, should be more thoroughly assessed for a wider range of inlet fluid velocities.

DOI: 10.1685/journal.caim.370

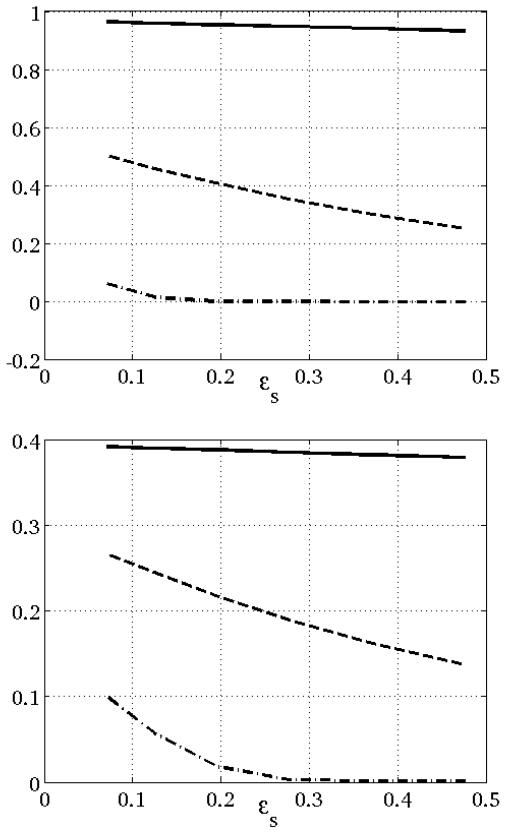

Figure 8. Maximum (solid line), minimum (dash-dotted line) and average (dashed line) values of c/c_0 (top) and ϵ (bottom) as functions of ϵ_s.

Acknowledgements.

The authors gratefully acknowledge Davide Colombo for his help in producing the numerical results illustrated in Sect. 4.

REFERENCES

1. B. Palsson and S. Bhatia, *Tissue engineering*, ch. Scaling up for ex vivo cultivation, pp. 223–243. Pearson Education, 2004.
2. A. J. E. Haj, M. A. Wood, P. Thomas, and Y. Yang, Controlling cell biomechanics in orthopaedic tissue engineering and repair, *Pathologie Biologie*, vol. 53, no. 10, pp. 581 – 589, 2005.
3. M. Raimondi, M. Moretti, M. Cioffi, C. Giordano, F. Boschetti, K. Laganà, and R. Pietrabissa, The effect of hydrodynamic shear on 3d engineered chondrocyte systems subject to direct perfusion, *Biorheology*,

vol. 43, no. 3-4, pp. 215–22, 2006.

4. N. Dunkelman, M. Zimber, R. Lebaron, R. Pavelec, M. Kwan, and A. Purchio, Cartilage production by rabbit articular chondrocytes on polyglycolic acid scaffolds in a closed bioreactor system, *Biotech. Bioeng.*, vol. 46, pp. 299–305, 1995.
5. D. Pazzano, K. Mercier, J. Moran, S. Fong, D. DiBiasio, J. Rulfs, S. Kohles, and L. Bonassar, Comparison of chondrogensis in static and perfused bioreactor culture, *Biotechnology Progress*, vol. 16(5), pp. 893–896, 2000.
6. T. Davisson, R. Sah, and A. Ratcliffe, Perfusion increases cell content and matrix synthesis in chondrocyte three-dimensional cultures, *Tissue Engineering*, vol. 8, no. 5, pp. 807–816, 2002.
7. M. Raimondi, F. Boschetti, L. Falcone, G. Fiore, A. Remuzzi, E. Marinoni, M. Marazzi, and R. Pietrabissa, Mechanobiology of engineered cartilage cultured under a quantified fluid-dynamic environment, in *Biomechanics and modeling in mechanobiology*, vol. 1, pp. 69–82, Berlin, Germany: Springer-Verlag, 2002.
8. M. Raimondi, F. Boschetti, L. Falcone, F. Migliavacca, A. Remuzzi, and G. Dubini, The effect of media perfusion on three-dimensional cultures of human chondrocytes: integration of experimental and computational approaches, *Biorheology*, vol. 41, no. 3-4, pp. 401–10, 2004.
9. A.-M. Freyria, Y. Yang, H. Chajra, C. Rousseau, M.-C. Ronzire, D. Herbage, and A. E. Haj, Optimization of dynamic culture conditions: Effects on biosynthetic activities of chondrocytes grown in collagen sponges, *Tissue Engineering*, vol. 11, no. 5-6, pp. 674–684, 2005.
10. L. Freed and G. Vunjak-Novakovic, Tissue engineering bioreactors, in *Principles of tissue engineering* (R. P. Lanza, R. Langer, and J. Vacanti, eds.), San Diego: Academic Press, 2000.
11. F. Guilak and C. Hung, *Basic orthopaedic biomechanics and mechanobiology*, ch. Physical regulation of cartilage metabolism, pp. 259–300. Lippincott Williams and Wilkins, 2005.
12. A. Grodzinsky, M. Levenston, M. Jin, and E. Frank, Cartilage tissue remodeling in response to mechanical forces, *Annual Review of Biomedical Engineering*, vol. 2, no. 1, pp. 691–713, 2000.
13. F. Silver, *Mechanosensing and Mechanochemical Transduction in Extracellular Matrix*, ch. Mechanochemical Sensing and Transduction, pp. 211–261. Springer US, 2006.
14. B. Obradovic, R. Carrier, G. Vunjak-Novakovic, and L. E. Freed, Gas exchange is essential for bioreactor cultivation of tissue engineered cartilage, *Biotechnol Bioeng.*, vol. 63(2), pp. 197–205, 1999.
15. B. Obradovic, J. H. Meldon, L. E. Freed, and G. Vunjak-Novakovic,

DOI: 10.1685/journal.caim.370

Glycosaminoglycan deposition in engineered cartilage: Experiments and mathematical model, *AIChE J.*, vol. 46, pp. 1547–5905, 2000.

16. M. Devarapalli, B. Lawrence, and V. Sundararajan, Modeling nutrient consumptions in large flow–through bioreactors for tissue engineering, *Biotechnol Bioeng*, vol. 103(5), pp. 1003–1015, 2009.
17. R. Bowen, Theory of mixtures, in *Continuum Physics* (e. A. C. Eringen, ed.), vol. 3, p. 11, Academic Press, 1976.
18. C. Marle, On macroscopic equations governing multiphase flow with diffusion and chemical reactions in porous media., *Int J Eng Sci*, vol. 20(5), pp. 643–662, 1982.
19. S. Whitaker, *The method of volume averaging. Theory and application of transport in porous media.* Kluwer Academic Publishers, 1999.
20. H. M. Byrne, J. R. King, D. L. S. McElwain, and L. Preziosi, A two-phase model of solid tumour growth, *Applied Mathematics Letters*, vol. 16, no. 4, pp. 567 – 573, 2003.
21. C. J. Galban and B. R. Locke, Analysis of cell growth kinetics and substrate diffusion in a polymer scaffold, *Biotechnology and Bioengineering*, vol. 65, no. 2, pp. 121–132, 1999.
22. B. D. Wood, M. Quintard, and S. Whitaker, Calculation of effective diffusivities for biofilms and tissues, *Biotech. and Bioeng.*, vol. 77, no. 5, pp. 495–514, 2002.
23. C. Chung, C. Chen, C. Chen, and C. Tseng, Enhancement of cell growth in tissue-engineering constructs under direct perfusion: Modeling and simulation, *Biotechnology and Bioengineering*, vol. 97, no. 6, pp. 1603–1616, 2007.
24. R. Sacco, P. Causin, P. Zunino, and M. T. Raimondi, A multiphysics/multiscale 2D numerical simulation of scaffold-based cartilage regeneration under interstitial perfusion in a bioreactor, *Biomechanics and Modeling in Mechanobiology*, 2010.
25. A. Quarteroni and A. Valli, *Numerical Approximation of Partial Differential Equations (2nd Ed.)*. New York: Springer-Verlag, 1997.
26. M. T. Raimondi, F. Boschetti, F. Migliavacca, M. Cioffi, and G. Dubini, Micro fluid dynamics in three-dimensional engineered cell systems in bioreactors, in *Topics in Tissue Engineering* (N. Ashammakhi and R. L. Reis, eds.), vol. 2, ch. 9, 2005.
27. M. Cioffi, F. Boschetti, M. T. Raimondi, and G. Dubini, Modeling evaluation of the fluid-dynamic microenvironment in tissue-engineered constructs: a micro-CT based model, *Biotechnol. Bioeng.*, vol. 93, no. 3, pp. 500–510, 2006.
28. S. Whitaker, Diffusion and dispersion in porous media, *A.I.Ch.E.Jl.*, vol. 13, pp. 420–427, 1967.

29. S. Whitaker, Flow in porous media i: a theoretical derivation of Darcy's law, *Transport in Porous Media*, vol. 1, pp. 3–25, 1986.

30. C. Hsu and P. Cheng, Thermal dispersion in a porous medium, *Int. J. Heat Mass Transfer*, vol. 33, no. 8, pp. 1587–1597, 1990.

31. D. Nield and A. Bejan, *Convection in Porous Media.* New York: Springer-Verlag, 1998.

32. J. Bear, *Dynamics of Fluids in Porous Materials.* New York: American Elsevier, 1972.

33. F. V. Parada, *Boundary conditions for the transport between multiphase media.* PhD thesis, Universidad Autonoma Metropolitana Unidad Iztapalapa, 2007.

34. C. J. Galban and B. R. Locke, Effects of spatial variation of cells and nutrient product concentrations coupled with product inhibition on cell growth in a polymer scaffold, *Biotechnology and Bioengineering*, vol. 64, no. 6, pp. 633–643, 1999.

35. D. E. Contois, Kinetics of bacterial growth: Relationship between population density and specific growth rate of continuous cultures, *J. Gen. Microbiol.*, vol. 21, pp. 40–50, 1959.

36. H. G. Roos, M. Stynes, and L. Tobiska, *Numerical methods for singularly perturbed differential equations.* Berlin Heidelberg: Springer-Verlag, 1996.

37. P. Ciarlet, *The Finite Element Method for Elliptic Problems.* Amsterdam: North Holland, 1978.

38. P. Hood and C. Taylor, Navier–Stokes equations using mixed interpolation, in *Finite Element Methods in Flow Problems* (J. T. Oden, R. H. Gallagher, O. C. Zienkiewicz, and C. Taylor, eds.), pp. 121–132, University of Alabama in Huntsville Press, 1974.

39. A. N. Brooks and T. J. R. . Hughes, Streamline upwind Petrov-Galerkin formulations for convection dominated flows with particular emphasis on the incompressible Navier-Stokes equations, *Comput. Meths. Appl. Mech. and Engr.*, vol. 32, pp. 199–259, 1982.

40. L. P. Franca, S. L. Frey, and T. J. R. . Hughes, Stabilized finite element methods: I. application to the advective–diffusive model, *Comput. Methods Appl. Mech.Engrg.*, vol. 95, pp. 253–276, 1992.

41. F. Galbusera, M. Cioffi, M. T. Raimondi, and R. Pietrabissa, Computational modelling of combined cell population dynamics and oxygen transport in engineered tissue subject to interstitial perfusion, *Computer Methods in Biomechanics and Biomedical Engineering*, vol. 10, no. 4, pp. 279–287, 2007.